Electrodynamics of the nodal metal state in weakly doped high-T_c cuprates

Y. S. Lee,[1,*] Kouji Segawa,[2] Z. Q. Li,[1] W. J. Padilla,[1,†] M. Dumm,[1,‡] S. V. Dordevic,[3] C. C. Homes,[3] Yoichi Ando,[2] and D. N. Basov[1]

[1]*Department of Physics, University of California at San Diego, La Jolla, California 92093-0319, USA*

[2]*Central Research Institute of Electric Power Industry, Komae, Tokyo 201-8511, Japan*

[3]*Department of Physics, Brookhaven National Laboratory, Upton, New York 11973, USA*

We report on the detailed analysis of the infrared (IR) conductivity of two prototypical high-T_c systems YBa$_2$Cu$_3$O$_y$ and La$_{2-x}$Sr$_x$CuO$_4$ throughout the complex phase diagram of these compounds. Our focus in this work is to thoroughly document the electromagnetic response of the nodal metal state which is initiated with only a few holes doped in parent antiferromagnetic systems and extends up to the pseudogap boundary in the phase diagram. The key signature of the nodal metal is the two-component conductivity: the Drude mode at low energies followed by a resonance in mid-IR. The Drude component can be attributed to the response of coherent quasiparticles residing on the Fermi arcs detected in photoemission experiments. The microscopic origin of the mid-IR band is yet to be understood. A combination of transport and IR data uncovers fingerprints of the Fermi liquid behavior in the response of the nodal metal. The comprehensive nature of the data sets presented in this work allows us to critically re-evaluate common approaches to the interpretation of the optical data. Specifically we re-examine the role of magnetic excitations in generating electronic self-energy effects through the analysis of the IR data in a high magnetic field.

I. INTRODUCTION

Recent experimental studies of weakly doped cuprates have revealed an enigmatic state: the nodal metal.[1–5] This state is realized with only a few holes introduced in parent antiferromagnetic (AF) insulators where doped materials still show AF ordering or the so-called spin-glass regime at low temperatures and extends throughout the notorious pseudogap region. Spectroscopic signatures of this electronic state include a Drude-like response in the optical conductivity[3,4] and a quasiparticle (QP) peak on the nodal "Fermi arc" seen in the photoemission data.[6] The electronic mobility and the Fermi velocity of nodal QP, as well as their optical effective mass, remain virtually unchanged as doping progresses to much higher carrier density where superconductivity is optimized.[1,2,7] All of these observations contradict a common characterization of the AF-ordered region of phase diagram as "antiferromagnetic insulator."

Carrier dynamics in the nodal metal is strongly influenced by unidirectional spin and/or charge self-organization effects commonly referred to as stripes.[8] Unambiguous manifestations of stripes can be found through experiments probing the anisotropy of conductivity within the nearly square CuO$_2$ planes.[9] Infrared (IR) experiments carried out with polarized light reveal the enhancement of optical conductivity along the "spin stripes" direction in La$_{2-x}$Sr$_x$CuO$_4$ (LSCO) (Refs. 3 and 9) and along the ripples of the electron density in the CuO$_2$ planes in YBa$_2$Cu$_3$O$_y$ (YBCO).[4]

The carrier density n in the nodal metal varies linearly with doping: a result that became established shortly after the discovery of high-T_c superconductors[10] and detailed in more recent studies.[1,11,12] An important consequence of the $n \propto x$ relationship is a dramatic suppression of the resistivity probed within the CuO$_2$ plane as one proceeds from antiferromagnetically ordered phases to overdoped metals. It is rather surprising that dynamical characteristics of charges including the electronic mobility,[1] the nodal Fermi velocity,[2] or quasiparticles optical mass m^{*}[7] reveal insignificant changes throughout the phases diagram.

In this paper we report on a detailed study of the nodal metal state in YBCO: a prototypical high-T_c superconductor carried out using untwinned single crystals for ten different dopings between $y=6.28$ and $y=7.00$. These new results unveil the evolution of the electromagnetic response as doping progresses from AF-ordered phase to superconducting materials. New data allow us to comprehensively test and re-examine common approaches in analyzing the electrodynamics of cuprates. We show that the IR signatures of the nodal metal involve a two-component conductivity: the Drude mode at low energies followed by a resonance in mid-IR. The Drude component can be attributed to the response of coherent QP residing on the Fermi arcs; the microscopic origin of the mid-IR band is yet to be thoroughly understood. The two-component conductivity extends to the pseudogap boundary in the phase diagram at T^{*}. We find similar trends in the response of the LSCO system and conclude that the nodal metal state is a hallmark of the electrodynamics of the pseudogap regime. In order to narrow down the range of possible microscopic interpretations of the mid-IR structure we have carried out studies of the $y=6.65$ single crystal in high magnetic field (**H**). These experiments allow one to assess the possible role of magnetic fluctuation in the QP dynamics. Our findings are at odds with the idea of the dominant role of magnetic resonance seen in neutron scattering experiments in mid-IR response.

This paper is organized as follows. In Sec. II we report on experimental details of crystal preparation, characterization, and reflectance measurements. The dc resistivity, the Hall coefficient, and the raw reflectivity data for YBCO de-

TABLE I. Summary on transition temperatures of the YBCO samples analyzed in this paper. Néel temperature T_N is determined from the c-axis resistivity measurement (Ref. 14). Superconducting transition temperature T_c is determined by the onset temperature of $\rho_{dc}(T)=0$.

y	6.28	6.30	6.35	6.40	6.43	6.50	6.55	6.65	6.75	7.00
T_N (K)	>300	230	80							
T_c (K)				2	13	31	48	60	65	92

twinned single crystals are also discussed in this section. Section III is devoted to the survey of the optical conductivity with variation of doping and temperature. Characteristic features of the conductivity are discussed in the context of the phase diagram of the YBCO system. Section IV is focused on the analysis of the optical conductivity in terms of two competing approaches: single-component and multicomponent descriptions. A simple two-component model is shown to grasp the gross trends in the evolution of the conductivity throughout the entire doping and temperature range. In Sec. V we investigate the transformation of the optical conductivity below T_c. It is found that the dominant contribution to the superconducting condensate originates from the coherent quasiparticles on the Fermi arc. In Sec. VI we discuss measurements in high magnetic fields carried out for $y=6.65$ crystal with the goal to address the role of the magnetic resonance in the CuO_2 plane optical conductivity of YBCO. Changes of reflectivity spectra with magnetic field are simulated within the framework of the electron-boson coupling theory and compared with experimental results. In Sec. VII, we analyze some of the implications of new experimental results focusing on common trends between the YBCO and LSCO series as well as on the possible origin of the mid-IR absorption. Summary and outlook of this work are presented in Sec. VIII.

II. EXPERIMENTAL DETAILS AND RAW DATA

We investigated detwinned YBCO single crystals with oxygen content $y=6.28$, 6.30, 6.35, 6.40, 6.43, 6.50, 6.55, 6.65, 6.75, and 7.00. A summary of the Néel temperatures T_N for AF-ordered samples and of superconducting transition temperatures T_c for superconducting specimens is given in Table I.[13,14] Single crystals were grown by a conventional flux method in Y_2O_3 crucibles and detwinned under uniaxial pressure at Central Research Institute of Electric Power Industry.[13] Note that the quality of these crystals is comparable to those grown in $BaZrO_3$ crucibles, as is evidenced by the thermal conductivity data below T_c.[15] Annealing under uniaxial pressure also aligns chains fragments along the b axis in nonsuperconducting YBCO ($y=6.28-6.35$). The typical sizes of the nearly rectangular samples are $\sim 1 \times 1.5$ mm^2 in the ab plane with the submillimeter thickness. Detwinned single crystals allow us to investigate the response of the CuO_2 plane (a axis) unperturbed by contributions due to the chain structures along the b axis. In this paper, we restrict our study to the a axis optical spectra; we reported on the electrodynamics associated with the chain segments in heavily underdoped YBCO in two other publications.[4,16]

The dc resistivity $\rho_{dc}(T)$ and Hall coefficient $R_H(T)$ curves of the YBCO samples studied in this paper are displayed in Fig. 1.[11,13] At moderately high T ρ_{dc} shows a metallic behavior in all samples including those that order antiferromagnetically ($y<6.40$) (top panel).[1] This metallic behavior persists well below T_N. At low T one can notice a negative slope of the resistivity in both nonsuperconducting samples ($y=6.28-6.35$) as well as in superconducting specimens ($y=6.40$ and 6.43). Resistivities for $y=6.65$ and 6.75 samples overlap between 70 K and 140 K; this is a peculiar behavior associated with the so-called 60 K-phase anomaly.[13] In the underdoped range the Hall coefficient does not show a strong T dependence and therefore data in the bottom panel of Fig. 1 can be used for obtaining a rough estimate of the carrier density from $R_H(T)$ ($R_H=1/ne$).

Reflectivity spectra $R(\omega)$ at nearly normal incidence were measured with polarized light at frequencies from 20 to 48 000 cm^{-1} and at temperatures from 10 to 293 K at University of California at San Diego. An *in situ* gold-coating technique was employed for reference spectra.[17]
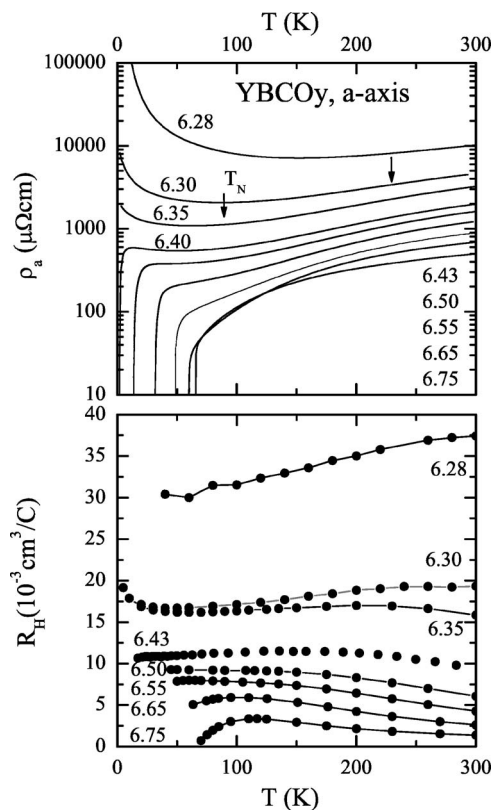

FIG. 1. (a) dc resistivity and (b) Hall coefficient curves for $y=6.28-6.75$ single crystals. The arrows represent T_N for AF samples. The T_N for $y=6.28$ is above 300 K.
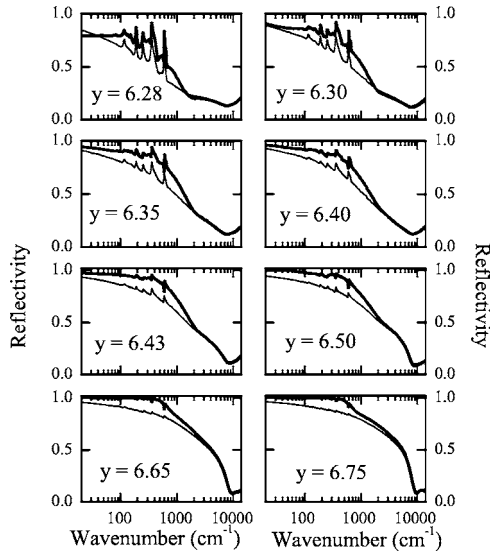
FIG. 2. Reflectance spectra for $y=6.28-6.75$ single crystals measured along the a axis at 10 K (thick lines) and 293 K (thin lines). For clarity, reflectance spectra are shown in the range from 0 to 1.02 on the vertical axis for highly reflective samples with $y \geqslant 6.43$.

Far-IR reflectance of actual gold films $R^{gold}(\omega)$ was evaluated from measurements of dc resistivity using the Hagen-Rubens formula and mid-IR and near-IR reflectivity of the gold coatings was directly determined using ellipsometric measurements. T dependence of $R^{gold}(\omega)$ has to be taken into account for calibration in far-IR range. Thus the obtained data for $R^{gold}(\omega)$ at various temperatures were used to generate absolute reflectivity for all studied samples.

In Fig. 2 we show $R(\omega)$ for polarization of the **E** vector along the a axis measured at 10 and 293 K. A common feature of $R(\omega)$ traces is their "metallic character:" all spectra reveal an increase of the absolute value with lowering ω starting from a "plasma minimum" at $\simeq 10\,000$ cm^{-1}. The magnitude of the reflectance in far-IR increases with doping so that the contribution of the transverse optical-phonon modes becomes less pronounced. With T decreasing, the low frequency $R(\omega)$ increases significantly, whereas the change in the mid-IR is fairly small. For $y=6.28$ and 6.30 where the low-T resistivity shows a semiconducting behavior below T_{Loc}; spectra measured at 10 and 80 K cross at the lowest frequencies (80 K data are not shown). As will be detailed in Sec. III, this latter effect is due to the modification of charge dynamics by disorder.

III. DOPING TRENDS IN THE OPTICAL CONDUCTIVITY

The complex optical conductivity spectra $\sigma(\omega)=\sigma_1(\omega)+i\sigma_2(\omega)$ were obtained from $R(\omega)$ using the Kramers-Kronig (KK) transformation. The KK-derived results are consistent with those determined independently by ellipsometry in the near-IR and visible regions. These results are presented in the left panels of Fig. 3 where we plot the a axis $\sigma_1(\omega)$ spectra at 10 and 293 K. For superconducting crystals we also show data at $T \sim T_c$. The sharp peaks below 700 cm^{-1}
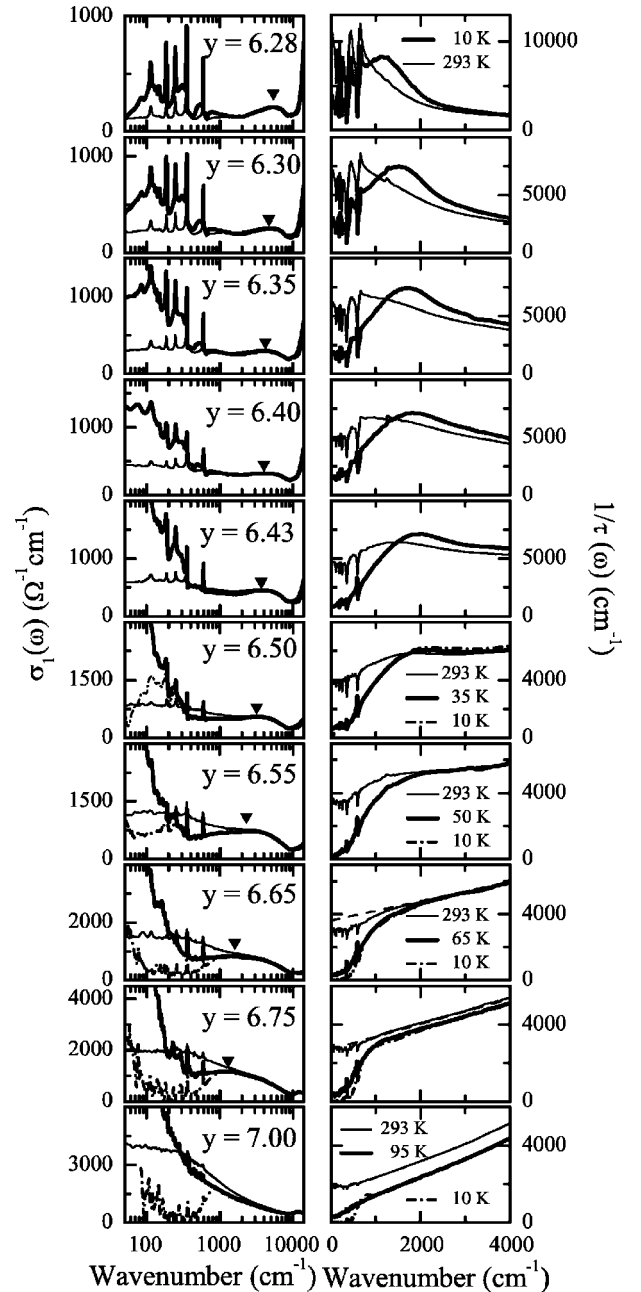

FIG. 3. Spectra of the a-axis conductivity $\sigma_1(\omega)$ (left panels) and of the scattering rate $1/\tau(\omega)$ (right panels) extracted from the extended Drude model as described in the text for a series of YBCO single crystals. Thick solid lines show the data at lowest temperature in the normal state: 10 K for nonsuperconducting crystals $y=6.28-6.40$ and $T \sim T_c$ for superconducting compounds $y=6.43-7.00$. The solid triangles in the left panels mark the positions of the mid-IR absorption bands. In right panles for $y=6.65$ and 6.75, the dashed lines represent the linear ω dependence.

are due to transverse optical-phonon modes. In all samples we find evidence for a charge-transfer (CT) gap near 10 000 cm^{-1}; this feature is especially evident in most weakly doped compounds, but can be recognized even in the data for the $y=6.75$ crystal. The intragap conductivity of all materials also reveals common patterns that become particularly clear in the low-T spectra (thick lines). We find
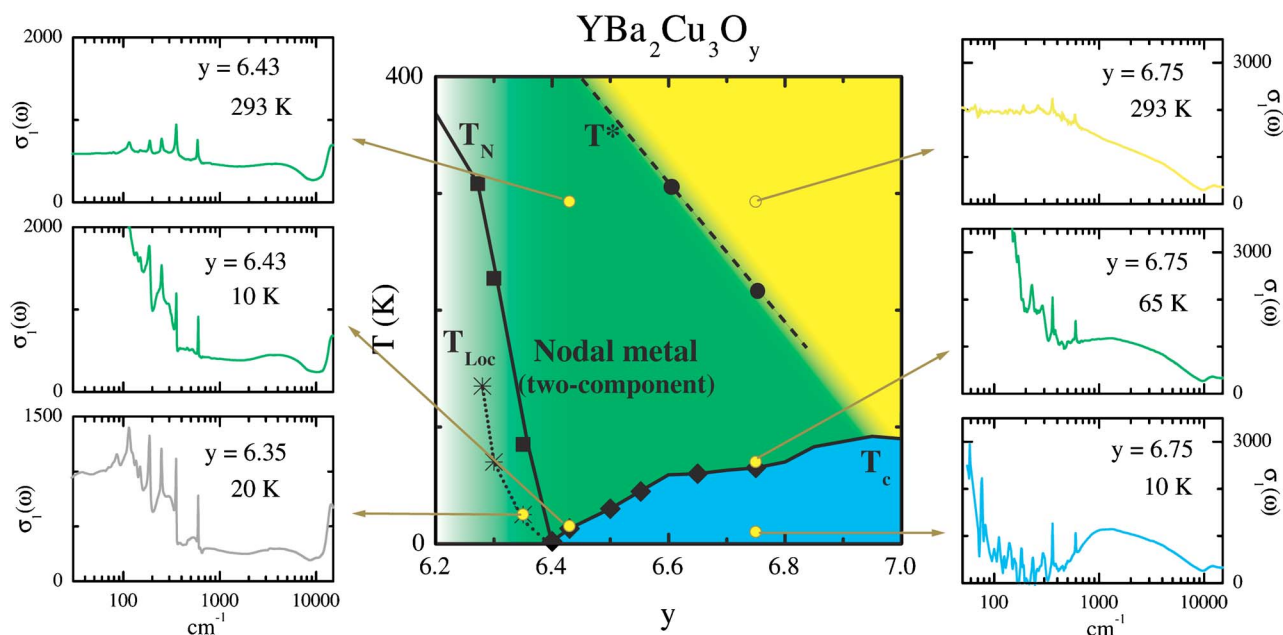
FIG. 4. (Color online) Mapping of the representative optical spectra to the phase diagram. The yellow circles represent y and T for the corresponding spectra. Black symbols represent characteristic temperatures of the samples studied in the paper. T_{Loc} is a crossover temperature signifying a semiconducting upturn in $\rho_a(T)$. It is noted that T_{Loc} is much below T_N, which indicates that the semiconducting behavior is unrelated to a long range of the AF-ordered state.

that the low-T spectra in the heavily underdoped region are composed of two separate absorption features: a coherent mode (at $\omega < 600$ cm^{-1}) followed by a mid-IR absorption at 0.5–0.6 eV.[4] The mid-IR structure is virtually T-independent, whereas the coherent mode significantly narrows at low T. As the doping increases the mid-IR absorption gradually shifts to lower frequency from ~ 5000 cm^{-1} in the $y=6.28$ sample down to ~ 1300 cm^{-1} for $y=6.75$, but still remains distiguishable from the well-developed coherent mode.

A remarkable result presented in Figs. 3 and 4 is a conventional Drude behavior of an antiferromagnetically ordered crystal with $y=6.35$.[4] (The details of the Drude fits are presented in Fig. 6.) This result conflicts with a common reference to weakly doped phases as "antiferromagnetic insulators" since the conventional Drude response is a standard characteristic of metallic transport. The weak upturn in $\rho_{dc}(T)$ at $T<20$ K (Fig. 1) is most likely caused by disorder-induced localization. Signatures of localization can be identified in the ω-dependence of the conductivity measured for samples with $y \leq 6.30$, where the coherent contribution to the conductivity reveals a peak at finite far-IR frequencies.[3] Importantly, the response of all crystals remains gapless down to the lowest ω as evidenced by a substantial spectral weight in the $\sigma_1(\omega)$ down to $\omega \to 0$. It is also found that at the lowest frequencies (~ 40–50 cm^{-1}) the optical conductivity is in good agreement with the ρ_{dc} values. This agreement holds at all temperatures. Based on this agreement with the transport data we conclude that no dramatic changes are likely to occur in the IR data at frequencies below our lower cutoff. For this reason we believe that the negative slope of the low-T resistivity in weakly doped YBCO is not due to the opening of the insulating gap. Instead we attribute this behavior to a

bandlike response even in lightly doped samples that is modified by weak localization.[18–21]

It is instructive to discuss the evolution of the conductivity spectra both with temperature and doping in the context of the phase diagram of YBCO system. The pseudogap boundary at T^* is associated with the formation of the partial (incomplete) gap in the spectrum of the low-energy excitations.[22] Spectroscopic signatures of the pseudogap are most clearly seen in the interplane c axis optical conductivity showing a depletion of the far-IR spectral weight below T^*.[23,24] Changes of the in-plane response probed in the polarization $\mathbf{E} \parallel CuO_2$ attributable to the pseudogap are much more subtle. These changes are usually discussed using the extended Drude formalism that we will introduce in Sec. IV. However both the comprehensive nature of the data set presented in Fig. 3 and the quality of these spectra allow one to identify important trends *directly* in $\sigma_1(\omega)$ spectra. One difference from the earlier studies[25,26] is that we are now confident to display T-dependent spectra up to 2 eV owing to both improvements in reflectance measurements and to availability of ellipsometric results in near-IR and visible ranges. At $T > T^*$ we observe a broad spectrum extending from $\omega = 0$ to the CT frequency (top-right panel of Fig. 4). This response can be characterized as single-component since multiple absorption features cannot be unambiguously singled out. Crossing the T^* boundary in Fig. 4 either vertically (by changing temperature at constant y) or horizontally (by changing doping at constant T) yields similar results. Indeed, two distinct absorption structures are affiliated with the entire green (gray) region of the phase diagram. These structures include a Drude mode at the lowest frequencies and mid-IR band. Similarities are especially clear when the low-T data are compared (the middle panels of Fig. 4). The
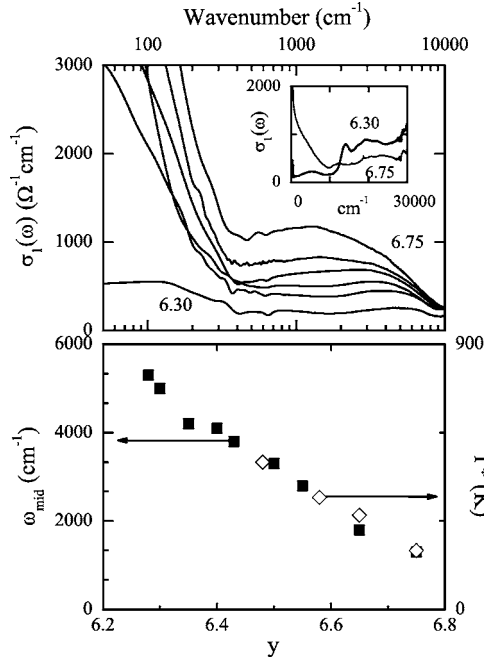
FIG. 5. (Top panel) Doping dependent $\sigma_1(\omega)$ at 10 K or at $T \simeq T_c$ for $y=6.30$, 6.35, 6.43, 6.50, 6.55, and 6.75. For clarity, the sharp phonon structures are removed. Inset shows the $\sigma_1(\omega)$ up to 30 000 cm^{-1} for $y=6.30$ and 6.75. (Bottom panel) Doping dependences of the peak position of mid-IR absorption ω_{mid} (solid square) and the pseudogap onset temperature T^* (open square) quoted from Ref. 22. The ω_{mid}/k_BT^* values are estimated to be 7–9.

main distinction in the latter spectra taken for $y=6.43$ and 6.75 compounds is in the frequency position of the mid-IR band at ω_{mid}. The softening of this feature with increasing doping is continuous as clearly seen in Figs. 3 and 5. As pointed out above, this two-component response is among the signatures of the nodal metal detected already in the AF sector of the phase diagram (bottom-left panel in Fig. 4). We therefore conclude that the nodal metal characteristics extend throughout both the AF and pseudogap regions of the phase diagram.

A conspicuous aspect of the phase diagram is that the electromagnetic response of YBCO is radically altered below the crossover temperature T^* (one-component $\rightarrow$ two-component transformation). This is surprising since the T^* boundary is rather "soft" given that no phase transition can be linked to T^*. At the same time, a true phase transition leading to the formation of the long-range antiferromagnetism does not trigger significant modifications in the optical data. This is also surprising in the context of a sharp onset of superconductivity near $y=6.40$. Our data for both YBCO and LSCO convincingly show that a certain minimum concentration of dopants is needed to initiate superconductivity. However, we are unable to recognize substantial distinctions between the response of AF-ordered and superconducting crystals apart from mild increase in the oscillator strength of both coherent and mid-IR contributions to $\sigma_1(\omega)$ spectra.

IV. UNDERSTANDING THE OPTICAL CONDUCTIVITY TRENDS: SINGLE-COMPONENT VERSUS MULTICOMPONENT DESCRIPTION

Two principal approaches are commonly used to describe the in-plane electromagnetic response of high-T_c cuprates: *multicomponent* and *one-component* model.[27] Within the latter approach it is assumed that the sole cause of the frequency dependence of $\sigma(\omega)$ is the response of itinerant carriers which acquire frequency dependent scattering rate $1/\tau(\omega)$ and frequency dependent mass $m^*(\omega)$ as the result of strong interactions in a system. The $1/\tau(\omega)$ and $m^*(\omega)$ spectra can be evaluated using the extended Drude model (EDM)

$$\sigma(\omega) = \frac{\omega_p^2}{4\pi} \times \frac{1}{1/\tau(\omega) - i\omega m^*(\omega)}, \qquad (1)$$

where ω_p ($\equiv 4\pi n e^2/m^*$) is the plasma frequency usually inferred from the integration of $\sigma_1(\omega)$ up to the energy of the CT excitation. The multicomponent approach [Eq. (2)] describes the functional form of the conductivity spectra using a set of (at least two) Lorentzian oscillators

$$4\pi\sigma(\omega) = \frac{\omega_{p,D}^2}{\Gamma_D - i\omega} + \frac{\omega_{p,L}^2 \omega}{i(\omega_c^2 - \omega^2) + \omega\Gamma_L}. \qquad (2)$$

In this equation the first term stands for the Drude response of the free carriers; $\omega_{p,D}$ is the Drude plasma frequency, and Γ_D is the scattering rate of the free carriers. The second term stands for the response of bound charges and has the form of a Lorentzian oscillator centered at ω_c with a plasma frequency $\omega_{p,L}$ and scattering rate Γ_L. Particular microscopic scenarios leading to these terms will be discussed in Sec. VII.

A debate on both merits and pitfalls of the two scenarios [Eqs. (1) and (2)] goes back to the early days of high-T_c superconductivity.[28,29] Here we will focus on the behavior of $1/\tau(\omega) = \omega_p^2/4\pi \times \text{Re}[1/\sigma(\omega)]$ pertaining to this debate and to the problem of the pseudogap. The right panels of Fig. 3 uncover the evolution of $1/\tau(\omega)$ with temperature and doping. The bottom panels presenting the $1/\tau(\omega)$ data for the $y=6.65$ and 6.75 crystals are in good agreement with the earlier results for underdoped YBCO.[25] $1/\tau(\omega)$ is nearly linear in ω at room temperature but shows a characteristic threshold structure near 500 cm^{-1} at $T < T^*$. It is this depression that is usually associated with the pseudogap state.[25,26,30,31] T^* is as high as 300 K for the $y=6.65$ sample but is reduced down to ~200 K for the $y=6.75$ compound. In the latter material we also find a parallel offset of the $1/\tau(\omega)$ for $T > T^*$. It has been also asserted that this form of $1/\tau(\omega)$ spectrum is indicative of coupling of QP to a (bosonic) mode occurring in the vicinity of the threshold structure.[32–35]

New unexpected features of the in-plane electrodynamics are uncovered by the data for heavily underdoped materials (top-right panels in Fig. 3). In these materials the $1/\tau(\omega)$ spectra at room temperature show a broad peak around 1000 cm^{-1}. With T decreasing, the scattering rate in far-IR is significantly suppressed, while the peak intensity is enhanced and the peak position shifts to higher frequencies. The non-
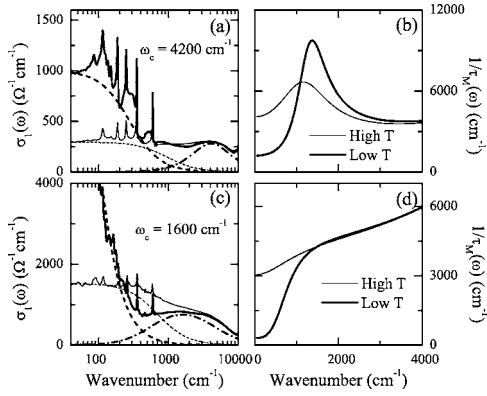
FIG. 6. Left panels: $\sigma_1(\omega)$ for (a) $y=6.35$ and (c) $y=6.65$ crystals. The dotted and the dot-dashed lines represent contributions due to the Drude mode and Lorentzian oscillator, respectively. The thick (thin) lines are for low (high) T. Fitting parameters are summarized in Table II. Right panels display modeled scattering rate $1/\tau_M(\omega)$ with fitting parameters for (b) $y=6.35$ and (d) $y=6.65$ crystals.
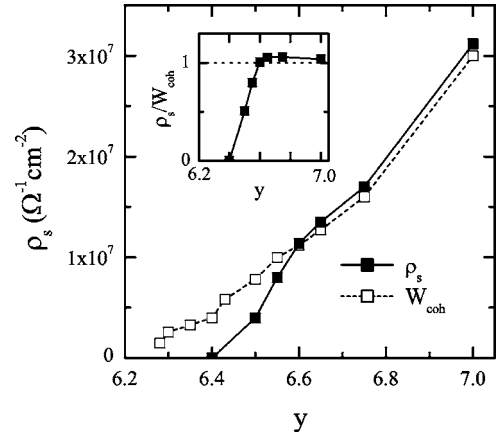

FIG. 7. Doping dependence of the superfluid density ρ_s (filled symbols) and the coherent spectral weight W_{coh} (open symbols) for a-axis data of a series of YBCO single crystals. Inset displays the ratio of ρ_s and W_{coh}.

monotonic form of the $1/\tau(\omega)$ observed in all crystals with $y<6.5$ is significant. Indeed, the negative slope (or peak structure) of the $1/\tau(\omega)$ at high frequencies is inconsistent with a single-component description of the electromagnetic response. This statement become readily apparent, for example, after a brief inspection of Allen's formula developed within the framework of the electron-boson scattering[36]

$$1/\tau(\omega) = \frac{2\pi}{\omega} \int_0^\omega d\omega'(\omega - \omega')\alpha^2 F(\omega') + \frac{1}{\tau_{\mathrm{imp}}}, \quad (3)$$

where $\alpha^2 F(\omega)$ is the electron-boson spectral function and $1/\tau_{\mathrm{imp}}$ is the impurity scattering. Because of the integral relationship between $1/\tau(\omega)$ and $\alpha^2 F(\omega)$ the slope of the scattering rate spectrum cannot be negative. Therefore, the non-monotonic dependence of $1/\tau(\omega)$ at low dopings clearly indicates a breakdown of the EDM analysis (or single-component analysis) to the heavily underdoped samples. This is hardly surprising given the fact that for the latter materials the two distinct absorption features are readily detected in the $\sigma_1(\omega)$ spectra. As the doping increases, the peak structures in the $1/\tau(\omega)$ spectra are suppressed and shift to higher frequencies. At doping $y \geqslant 6.5$ the peaks disappear from $1/\tau(\omega)$ making the slope in the $1/\tau(\omega)$ positive at all frequencies. A suppression in the far-IR $1/\tau(\omega)$ at lower T is

TABLE II. Summary of parameters for two-component model spectra $\sigma_M(\omega)$ and $1/\tau_M(\omega)$ spectra shown in Fig. 6. $\omega_{p,D}$ is the plasma frequency and Γ_D is the scattering rate for coherent mode; $\omega_{p,L}$ is the plasma frequency, Γ_L is the width, and ω_c is the position of the Lorentzian oscillator; $\omega_{p,M}$ is the total plasma frequency for $1/\tau_M(\omega)$. All parameters are given in cm^{-1}. Data in parentheses are for the low-T spectra (thin lines in Fig. 6).

y	$\omega_{p,D}$	Γ_D	$\omega_{p,L}$	ω_c	Γ_L	$\omega_{p,M}$
6.35	4100	280(950)	10850	4200	7000	8500
6.65	8000	60(700)	15000	1600	5000	18000

observed at all the dopings and merely reflects the narrowing of the coherent component in the conductivity data.

We will now demonstrate that the gross features of both $\sigma_1(\omega)$ and $1/\tau(\omega)$ spectra described above can be qualitatively reproduced within a two-component scenario for the electromagnetic response. We modeled the coherent contribution to the conductivity using the Drude formula with constant scattering rate Γ_D: whereas mid-IR absorption was accounted for with a single Lorentzian oscillator [Eq. (2)]. Separate contributions due to these two components are displayed with the dotted and dot-dashed lines in the left panels of Fig. 6. The corresponding form of the $1/\tau(\omega)$ spectra is presented in the right panels. First, we fitted the experimental $\sigma_1(\omega)$ for $y=6.35$ with the form of Eq. (2). Table II summarizes the fitting parameters. The parameters of the mid-IR contribution remained unchanged for modeling both the 293 K and 10 K data; the width of the Drude contribution was reduced to account for the narrowing of the coherent mode in the low-T spectra. As clearly seen in Fig. 6(b), the modeled scattering rate $1/\tau_M(\omega)$ reasonably reproduces the experimental data (right panel for $y=6.35$ in Fig. 3) including the broad peak structure and its T-dependence. We believe this outcome of the fitting procedure is rather natural since the two-component absorption is evident in the heavily underdoped region directly in the conductivity data.

Encouraged by the success of the two-component description of the data at very low dopings we applied Eq. (2) to model the spectra obtained for the $y=6.65$ crystal. We found that the frequency dependence of the modeled spectra $1/\tau_M(\omega)$ as well as their temperature dependence reproduce the key characteristic features of the experimental data in the pseudogap state (right panel for $y=6.65$ in Fig. 3). Naturally, the low frequency suppression of $1/\tau(\omega)$ is associated with the development and narrowing of the coherent mode. Only a minute T-dependence of $1/\tau(\omega)$ at frequencies above 500 cm^{-1} is accounted for by the mid-IR band which is essentially independent of temperature. We wish to emphasize nearly linear frequency dependence of the modeled $1/\tau(\omega)$ spectra in Fig. 3. This frequency dependence is often re-
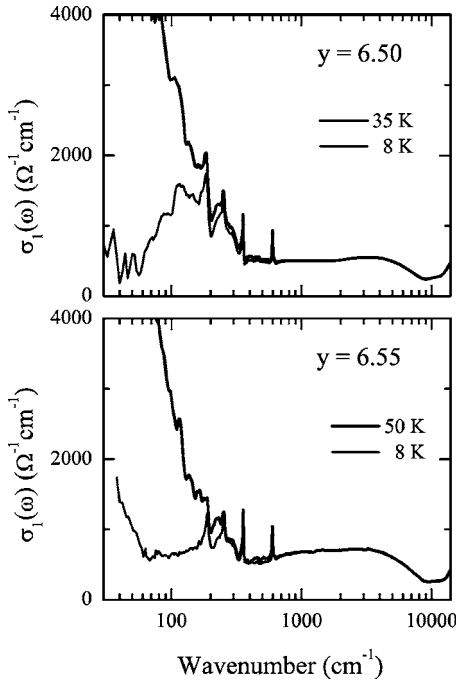
FIG. 8. Spectra of the a-axis conductivity $\sigma_1(\omega)$ for $y=6.50$ (top panel) and 6.55 (bottom panel) at $T \ll T_c$ (thin lines) and $T \sim T_c$ (thick lines).

garded as one of the most anomalous features of the normal state response of high-T_c superconductors. Our modeling shows that this may be a trivial outcome of the two-component character of the electromagnetic response. Note that in these calculations we employed the simplest model possible: one Lorentzian oscillator and a Drude mode with the single temperature-dependent parameter Γ_D. Obviously, improved fits can be obtained with more flexibility in the choice of the parameters. Nevertheless, it became possible to reproduce all important trends in the data using this simplest approach. We therefore conclude that the two-component model offers a sufficiently accurate description of the totality of experimental data including the response in the pseudogap state whereas the single-component approach clearly breaks down for doping below $y < 6.5$.

V. NODAL METAL IN THE SUPERCONDUCTING STATE

We now focus on the transformation of the optical conductivity below T_c. A salient feature of all superconducting crystals is a depression of $\sigma_1(\omega)$ in far-IR region at $T < T_c$ with the transfer of the "missing" spectral weight to superconducting δ peak at $\omega = 0$. This is in accord with earlier experimental work reviewed in Ref. 27. Infrared experiment enables reliable extraction of the superfluid density ρ_s from the optical constants.[37] In Fig. 7 we plot the doping dependence of the superfluid density obtained for the series of samples that we have investigated. One finds that ρ_s does not exceed the coherent contribution to the conductivity W_{coh}. The latter weight can be evaluated from integration of the conductivity up to 600 cm^{-1} [$W_{coh}=8 \times N_{eff}(\omega_c)=8 \times \int_0^{\omega_c} \sigma_1(\omega)d\omega'$, where $\omega_c=600$ cm^{-1}]: the frequency range

where the coherent component dominates in the optical response.

One interesting observation pertains to the frequency dependence of the $\sigma_1(\omega)$ for $y=6.65$ and 6.75 obtained just above T_c and at 10 K. The form of these spectra is very similar and the only difference is in the diminished spectral weight in the 10 K data fully accounted for by the area under the δ function.[38,39] New results reported here for even lower dopings: $y=6.50$ and 6.55 (Fig. 8) uncover several unexpected features. We present these spectra on the log scale in order to clearly display both the coherent contribution to the conductivity as well as mid-IR band. Notably, the two absorption structures are well separated, one from each other at these low dopings. This circumstance allows one to evaluate the role of both of these conductivity channels in the formation of superconducting condensate through the examination of spectral features rather than through the evaluation of the integrated spectral weight as in Fig. 7. The superconducting state spectra show that the spectral weight associated with the coherent component has been significantly diminished. Changes of the optical conductivity are primarily confined to the frequency range determined by the magnitude of the scattering rate in the $T \sim T_c$ curves. We do not observe any significant depletion of the conductivity associated with the mid-IR band at $T < T_c$. We therefore conclude that the dominant contribution to the superconducting condensate originates from the coherent quasiparticles on the Fermi arc.

In the superconducting state spectra plotted in Fig. 8 one can identify a gap like threshold structure in $\sigma_1(\omega)$ at ~ 100 cm^{-1} for $y=6.50$ crystal and at ~ 220 cm^{-1} for $y=6.55$ sample. These features are not seen at $T \gtrsim T_c$ and gradually develop with temperature lowering below the critical value. We assign this structure with superconducting energy gap. This assignment is warranted since these low-energy structures are well separated from all other absorption features. We also point out that the superconducting state conductivity remains finite down to the lowest energies. This is in the qualitative agreement with the expected theoretical behavior for dirty d-wave superconductors.[40] Alternatively, finite residual conductivity below the superconducting gap can be attributed to the tail of mid-IR band extending down to the lowest frequencies and/or inhomogeneous superconducting condensate.[41]

VI. MAGNETIC RESONANCE IN THE IN-PLANE CHARGE DYNAMICS OF YBCO

An important aspect of charge dynamics of cuprates is the possibility of QPs coupling to collective modes. A well-known example is the so-called Holstein bands arising in systems with strong electron-phonon interaction.[36,42–44] It was suggested early on that deviations of the in-plane optical conductivity of cuprates from conventional Drude form may originate from coupling to a bosonic mode.[45] Later analysis of the $\sigma(\omega)$[32,33,35,46] has indicated that the relevant mode in cuprates may be related to the so-called 41 meV magnetic resonance[47,48] observed in neutron scattering experiments. One appeal of the strong coupling approach is in its well-defined predictions, not only for IR experiments,[32,34] but also
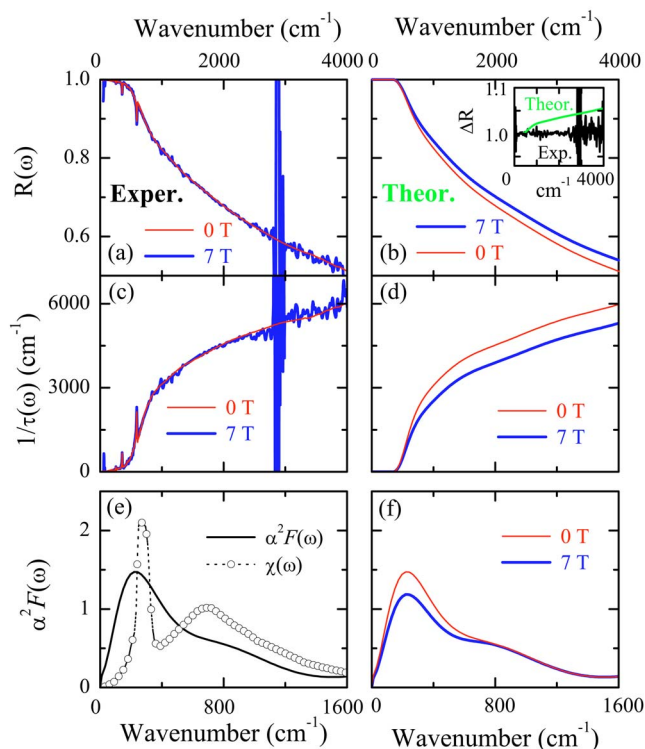
FIG. 9. (Color online) Low-temperature reflectance spectra (top) $R(\omega)$, (middle) $1/\tau(\omega)$ spectra, and (bottom) $\alpha^2F(\omega)$ data for y =6.65 YBCO single crystal at all 5 K. Red (thin) lines: $\mathbf{H}=0T$; blue (thick) lines: $\mathbf{H}=7T$. Left panels: experimental results. Right panels: model spectra calculated using the protocol described in the text. Inset in (b): $\Delta R(\omega,\mathbf{H})=R(\omega,7\ T)/R(\omega,0\ T)$. Sharp spikes in the high-field spectra are due to absorption in the windows of our cryostat. To calculate $\alpha^2F(\omega)$ we used $\Delta=180$ cm^{-1}. Calculations follow the procedure proposed in Ref. 57, with the 20% suppression of the resonance near 250 cm^{-1}. In (e) the $\alpha^2F(\omega)$ data extracted from the $\mathbf{H}=0T$ and $7T$ spectra are nearly identical. Also shown with open symbols in panel (e) is the spin susceptibility $\chi(\omega)$ from the INS data reported in Ref. 58 for y=6.6 (T_c=62.7 K) single crystal. The $\chi(\omega)$ spectrum is similar to the experimental result for $\alpha^2F(\omega)$ obtained from the inversion of IR data.

for data generated with other spectroscopic techniques including angle-resolved photoemission spectroscopy (ARPES)[49,50] as well as tunneling.[51,52] At least in the case of the optimally doped YBCO and Bi$_2$Sr$_2$CaCu$_2$O$_{8+\delta}$ (Bi2212) superconductors this analysis indeed provides a consistent account of the above mentioned spectroscopies based on the idea of QP coupling to a magnetic resonance. Recently, the role of magnetic resonance in QPs dynamics has been challenged. An examination of ARPES experiments has suggested that the totality of data is better described in terms coupling to phonons[53] and not to magnetic excitations. This claim is not supported by the IR studies of isotopically substituted YBCO, which show no isotope effect for the feature in question.[54,55]

Insights into strong-coupling effects may be gained from studies of the QP dynamics in the magnetic field. The rationale for this approach is provided by the work of Dai *et al.* who discovered that the intensity of the magnetic resonance
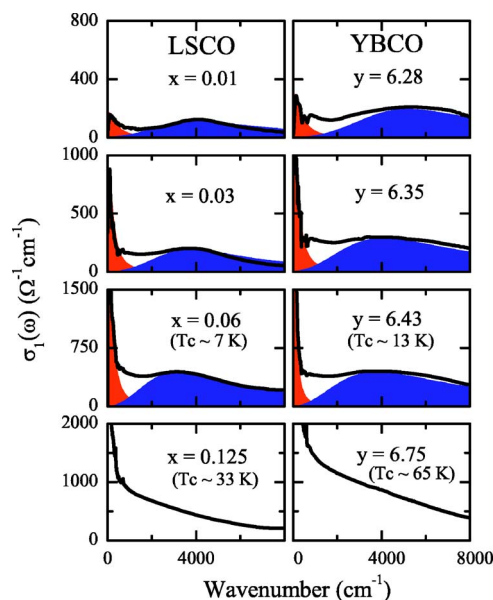

FIG. 10. (Color online) Evolution of the optical conductivity with doping in LSCO (left panels) and YBCO (right panels) series from Ref. 7. Data at 10 K are presented for nonsuperconducting crystals; data at $T \simeq T_c$ are shown for superconducting materials (at $T \simeq T^*$ for y=6.75). For clarity, phonons were removed from all spectra by fitting them with the Lorentzian oscillators. The response of weakly doped samples shows a Drude-like behavior at low frequencies followed by a resonance in mid-IR. Red (light gray) and blue (dark gray) areas represent the Drude and mid-IR absorption modes in Eq. (2), respectively.

in the y=6.6 YBCO crystal (T_c=62.7 K) is suppressed by 20% in 6.8 T field applied along the c axis.[56] Other candidate excitations including phonons, or the continuum of spin fluctuations, are unlikely to be influenced by a magnetic field of similar modest magnitude. For this reason an exploration of the field-induced modifications of the electronic self-energy enables a direct experimental inquiry into the role of the magnetic resonance in QP properties and, on a more general level, into an intricate interplay between superconductivity and magnetism in cuprates.

In order to quantify the magnitude of possible $\mathbf{H}$-induced changes in the reflectivity spectra we adopted the following procedure. We first extracted the spectral function $\alpha^2F(\omega)$ from the zero-field data for y=6.65. The detailed method is published elsewhere.[57] An extracted spectrum shows fair agreement with experimental results for the spin susceptibility $\chi(\omega)$ obtained from inelastic neutron scattering (INS) experiments [open symbols in Fig. 9(e)].[58] Specifically, both the peak at 250 cm^{-1} and a broad background of the INS data is reproduced through this analysis. We then reduced the intensity $\alpha^2F(\omega)$ by 20% without modifying the broad background in accord with INS measurements.[56] Using the spectral function with the suppressed intensity we calculated $1/\tau(\omega,7T)$,[57] and also $m^*(\omega,7T)$ with the help of Kramers-Kronig analysis. Finally, a combination of $1/\tau(\omega,7T)$ and $m^*(\omega,7\ T)$ allowed us to generate the reflectance spectrum $R(\omega,7\ T)$ [blue (thick) line in Fig. 9(b)]. Comparing this final output of modeling with the experimental curve for $\mathbf{H}$

=0 one finds that the effect of the applied magnetic field is rather small in the far-IR but exceeds 5% at frequencies above 800 cm^{-1}. Moreover, anticipated changes of reflectance exceed the conservative estimate for the uncertainty of $R(\omega, \mathbf{H})$ in a new apparatus we have developed for infrared magneto-optics[59] and therefore could be readily detected.

Representative results are displayed in Fig. 9. Here we plot the raw reflectance spectra measured at $T=5$ K for $y=6.65$ crystals. The spectra are in good agreement with the earlier studies of YBCO with similar oxygen content.[25] In our magneto-optics apparatus we are capable of measuring the absolute values of reflectivity in the magnetic field.[59] For $y=6.65$ system we found that the field-induced changes of the reflectivity are negligibly small either under zero-field cooling or under in-field cooling conditions. The same instrument was successfully used to monitor transitions between the Landau levels in graphite which produce only weak changes of $R(\omega)$ comparable to anticipated effect in YBCO.[59] We also repeated measurements for $y=6.50$ crystal and did not detect significant field-induced changes of reflectance in mid-IR. These results call for a revision of the prominent role of magnetic excitations in QPs dynamics.

VII. DISCUSSION

A. Two-component quasiparticles dynamics of the nodal metal and the pseudogap crossover

The key experimental finding of this work is that the gross features of the low-temperature electrodynamics in YBCO are adequately described within the two-component model [Eq. (2)]. This simple description holds throughout an extended region of the phase diagram from AF-ordered phases to the d-wave superconductor. The separation between the coherent Drude contribution to the conductivity and mid-IR band is most evident in the low-T response at very low dop-
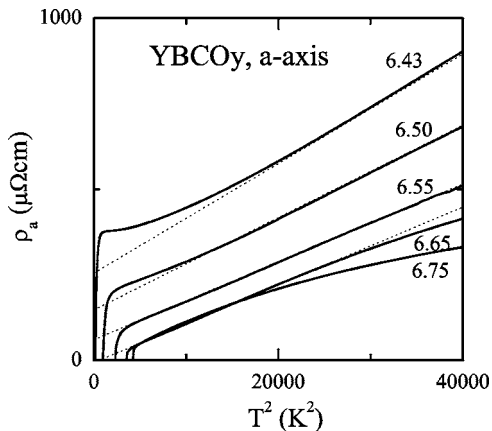

FIG. 11. T^2-dependence in dc resistivity $\rho_{dc}(T)$ in the YBCO series. The T^2 dependence is evident in the data below the T^* temperature. Even in heavily underdoped region $\rho_{dc}(T)$ exhibits T^2 dependence at moderately high temperatures. It is noted that the cotangent of the Hall angle, $\cot \Theta_H$, also shows the T^2 dependence in the corresponding region, which implies that the scattering rate should follow the T^2 dependence. For detailed discussion, see (Ref. 12).

ings. This aspect of electrodynamics is not specific to YBCO but is also common to the LSCO system[7,60] as well as for the electron-doped $Nd_{2-x}Ce_xCuO_4$ system.[61–63] As doping increases the spectral weight associated with both the coherent component and mid-IR band is enhanced (Fig. 10). Moreover, the mid-IR band systematically softens with increasing doping. The net result of these effects is that the two contributions merge and can no longer be separated beyond a certain doping level ($y > 6.75$ in YBCO and $x > 0.125$ in LSCO). We therefore conclude that the doping dependent evolution of optical spectra appears to reflect a generic property of cuprates.

Our experiments unequivocally show that at the pseudogap boundary of the phase diagram the charge dynamics of the CuO_2 plane experiences a crossover from a single-component type to two-component response of the nodal metal. Moreover, we find that at $T < T^*$ both transport and spectroscopic properties are consistent with the Fermi liquid (FL) theory.[64] This conjecture is supported by the Drude frequency dependence of the optical conductivity as well as by the T^2 form of the resistivity[12] plotted in Fig. 11. A prerequisite for the FL theory is well-defined quasiparticle excitations. The existence of such quasiparticles at $T < T^*$ is in accord with relatively large values of the electronic mean free path extracted from the analysis of the coherent component in the conductivity.[4] Further evidence for well-defined quasiparticles at $T < T^*$ is provided by observations of bilayer splitting effects both by ARPES[65] and by IR studies of the c-axis response.[66] Thus the totality of the experimental data suggests the Fermi liquid nature of the nodal metal.

Attributes of the FL dynamics of the nodal metal are most vivid in the temperature-doping parameter space where the coherent contribution is energetically separated from the incoherent mid-IR band. Photoemission experiments for the LSCO system conclusively show that this regime is realized when most of the Fermi surface is gapped and the only remaining portion is the arc formed around the nodal points.[6,67,68] The FL hallmarks can no longer be identified when the two-component behavior is terminated at the pseudogap boundary and the large Fermi surface is recovered. A corresponding feature of the optical data is the merger between Drude and mid-IR contributions, which is adequately described with the anomalous ω-dependence in $1/\tau(\omega)$, referred to as non-Fermi liquid.[28,69] Hall measurements for LSCO show a dramatic enhancement of the effective number of carriers participating in transport at the same boundary. In the earlier publications we have established a quantitative consistency between IR and Hall data.[7,12] Unfortunately, ARPES and high-temperature resistivity and/or Hall data are available only for LSCO system. However, close similarity between IR results for both LSCO and YBCO (Fig. 10) prompt us to conclude that the above trends may be reflecting intrinsic properties of weakly and moderately doped CuO_2 planes that are valid irrespective of a particular host material.

B. The origin of mid-IR band

The discussion in the previous subsection shows that the mid-IR band universally found in all high-T_c superconduct-

ors is intimately involved in the pseudogap phenomenology and specifically in transport properties at high temperatures.[7,12] Moreover, the softening of the mid-IR band with doping resembles the decrease of pseudogap temperature T^* as shown in the bottom panel of Fig. 5. In view of these preeminent roles of the MIR resonances it is prudent to inquire into the physics underlying this absorption feature. The form of the $1/\tau(\omega)$ spectra for weakly doped YBCO resembles that of systems with spin density and/or charge density wave.[31,70] This is a likely possibility given overwhelming evidence for spin and/or charge self-organization effects in weakly doped phases.[71] Recently, charge ordering patterns have been directly detected using scanning tunneling spectroscopy.[72,73] If the position of the mid-IR is chosen to characterize the magnitude of the electronic gap we find that $\omega_{mid} = 7\text{–}9\ k_B T^*$. This ratio is quite common for charge density wave states in solids.[74]

Several other possible scenarios for mid-IR band are worthy of our attention. A detailed analysis of the electronic structure of doped Mott insulators predicts several forms of bound states within the Mott-Hubbard and/or charge transfer gaps.[75] Then interband transitions involving these states may give rise to the observed effects in mid-IR. Recent ARPES results have reported that apart from the Fermi arc in the nodal region, the so-called flat band is formed around $(\pi, 0)$ of Brillouin zone at ~ -0.2 eV in heavily underdoped region and rises up to the Fermi level with the increased doping.[6,67] Interestingly, this doping dependence of the flat band is reminiscent of the softening of the mid-IR absorption. A different view on the nature of the mid-IR structure is given by Lorenzana and Sawatzky who argued that this feature is due to a quasibound state of two magnons coupled to an optical phonon.[76] Alternatively, the multi-component response including the mid-IR absorption might be attributed to the real space electronic inhomogeneity occurring due to embedding of metallic regions in an insulating host. Near the percolation threshold the optical conductivity of such a system shows a Drude response at low energies followed by a featureless background.[77–79] Yet another possibility is that the mid-IR absorption is produced by an incoherent band formed by the strong interaction of carriers with phonons[80] or spin fluctuation.[81] Finally, Leggett[82] and Turlakov[83] discussed the "plasmonic" nature of the mid-IR spectral feature. Within this latter scenario sizable changes in mid-IR spectra below T_c were predicted.[82] Experimentally, the temperature dependence of the mid-IR absorption is rather weak.[84] While further studies on the origin of the mid-IR absorption are needed, our findings strongly suggest that any explanation should take into account the correlation between the formation of the mid-IR absorption and the development of the pseudogap.

C. Self-energy effects in the quasiparticles dynamics

As pointed out in Sec. VI, reflectivity measurements performed in $\mathbf{H} \| c$ field do not show noticeable changes at the mid-IR frequencies calling for a critical re-examination of the roles of magnetic excitations in quasiparticle dynamics. Specifically, IR data reported in Fig. 9 challenge the rel-

evance of the resonance detected in the INS experiments to the electronic self-energy effects in mid-IR. An issue of whether or not the magnetic mode seen by the INS is capable to seriously impact the electronic self-energy in view of only small intensity of the resonance has been contested in the literature.[34,85,86] Our new results reported in Fig. 9 in conjunction with the INS experiments in high magnetic field challenge a preeminent role of magnetic resonance in electrodynamics of cuprates. More importantly, the self-energy interpretation of the IR data or the single-component approach appears to be in conflict with the main experimental finding of this work: the two-component nature of the electromagnetic response. It is therefore imperative to take into account this other contribution before inquiring into the role of self-energy in the coherent component of the conductivity.

As a note of caution it must be stressed that marked effects are not necessarily expected if the magnetic resonance broadens in the applied field. Since it is the integrated weight of the magnetic mode that is relevant for self-energy a simple smearing of the resonance is unlikely to significantly modify IR data. In this context we emphasize that INS results of Dai *et al.* suggest a reduction of the intensity of the mode and not its broadening.[56] If this latter behavior is confirmed by future neutron studies, our observed behavior is incompatible with the spin exciton interpretation of the INS resonance mode.

VIII. SUMMARY AND OUTLOOK

We investigated the electromagnetic responses of a prototypical high-T_c cuprate YBCO in a broad region of the phase diagram from the AF to the pseudogap state ($y = 6.28\text{–}6.75$). We focused on the analysis of the nodal metal phase that is characterized by a clear energy separation between the low-energy electronic states responsible for Drude conductivity and higher energy excitations producing mid-IR structure in the optical data. We emphasized close parallels in the IR data for YBCO and LSCO systems and concluded that the two-component characteristics may be generic for high-T_c cuprates. At least in the case of LSCO, the two-component nature of the electronic excitations is also consistent with both the ARPES and transport results.

A combination of transport and IR experiments has allowed us to identify several hallmarks of the Fermi liquid in the properties of the nodal metal. Interestingly, this rather conventional electronic behavior characterized with the high electronic mobility[1] and relatively low effective mass[7] extends to AF-ordered phases. These latter findings clearly show that the transition from a nodal metal to a Mott insulator is of "vanishing carrier number."[87] The above experiments also suggest that transport in nodal metals may be governed by excitations topologically compatible with an antiferromagnetic background. Many of the doping trends reported here are consistent with the projected wave functions approach.[88] One conjecture reconciling anomalous trends seen in weakly doped cuprates is that the local environment of mobile charges in these systems remains unaltered with doping and it is only the phase space occupied by hole rich regions that is progressively increasing.

We show that the pseudogap state in the generic phase diagram is associated with a crossover from the two-

component conductivity of a nodal metal to the single component response at $T > T^*$. In the vicinity of the pseudogap boundary the effective number of charge carriers contributing to transport and optics is enhanced.[7,12] This indicates that the functional form of the dc resistivity of cuprates $\rho_{dc}(T)$ is governed not only by the relaxation processes but also by temperature-dependent number of carriers. Even though the mid-IR band is contributing to transport at high temperature, the low-temperature properties of cuprates are dominated by nodal quasiparticles. In superconducting crystals the vast majority of the superfluid spectral weight is produced by condensation of nodal quasiparticles.

High-field magneto-optics experiments pose challenges for the interpretation of the IR spectra in terms of fermionic self-energy effects prompted by coupling of quasiparticles to a neutron resonance. In view of the two-component response documented here it is imperative to take into account the mid-IR contribution before the low-frequency data is employed to search for strong coupling effects. However, this task is connected with ambiguous procedures to remove the mid-IR contribution from the data. We therefore have not attempted this analysis here. We note that the success of a simple Drude plus Lorentzian description of the data (Fig. 6) indicates that the self-energy effects in optics may be rather weak. It is therefore of interest to re-examine the self-energy correction in the results obtained with other spectroscopies. Measurements in the magnetic field are of high interest in this context. While it may be impossible to carry out such experiments in the case of photoemission studies, tunneling measurements appear to be well suited for this task.

*Present address: Spin Superstructure Project, ERATO, JST, c/o AIST Tsukuba central 4, 1-1-1 Higashi, Tsukuba 305-8562, Japan.

†Present address: Los Alamos National Laboratory, MSK764, MST-10, Los Alamos, NM 87545, USA.

‡Present address: Physikalishes Institut, Universität Stuttgart, 70550 Stuttgart, Germany.

[1] Yoichi Ando, A. N. Lavrov, Seiki Komiya, Kouji Segawa, and X. F. Sun, Phys. Rev. Lett. **87**, 017001 (2001).

[2] X. J. Zhou, T. Yoshida, A. Lanzara, P. V. Bogdanov, S. A. Kellar, K. M. Shen, W. L. Yang, F. Ronning, T. Sasagawa, T. Kakeshita, T. Noda, H. Eisaki, S. Uchida, C. T. Lin, F. Zhou, J. W. Xiong, W. X. Ti, Z. X. Zhao, A. Fujimori, Z. Hussain, and Z.-X. Shen, Nature (London) **423**, 398 (2003).

[3] M. Dumm, Seiki Komiya, Yoichi Ando, and D. N. Basov, Phys. Rev. Lett. **91**, 077004 (2003).

[4] Y. S. Lee, Kouji Segawa, Yoichi Ando, and D. N. Basov, Phys. Rev. B **70**, 014518 (2004).

[5] Mike Sutherland, D. G. Hawthorn, R. W. Hill, F. Ronning, S. Wakimoto, H. Zhang, C. Proust, Etienne Boaknin, C. Lupien, Louis Taillefer, Ruixing Liang, D. A. Bonn, W. N. Hardy, Robert Gagnon, N. E. Hussey, T. Kimura, M. Nohara, and H. Takagi, Phys. Rev. B **67**, 174520 (2003).

[6] T. Yoshida, X. J. Zhou, T. Sasagawa, W. L. Yang, P. V. Bogdanov, A. Lanzara, Z. Hussain, T. Mizokawa, A. Fujimori, H. Eisaki, Z.-X. Shen, T. Kakeshita, and S. Uchida, Phys. Rev. Lett. **91**, 027001 (2003).

[7] W. J. Padilla, Y. S. Lee, M. Dumm, G. Blumberg, S. Ono, Kouji Segawa, Seiki Komiya, Yoichi Ando, and D. N. Basov, Phys. Rev. B (to be published).

[8] N. Ichikawa, S. Uchida, J. M. Tranquada, T. Niemöller, P. M. Gehring, S.-H. Lee, and J. R. Schneider, Phys. Rev. Lett. **85**, 1738 (2000).

[9] Yoichi Ando, Kouji Segawa, Seiki Komiya, and A. N. Lavrov, Phys. Rev. Lett. **88**, 137005 (2002).

[10] H. Takagi, T. Ido, S. Ishibashi, M. Uota, S. Uchida, and Y. Tokura, Phys. Rev. B **40**, 2254 (1989).

[11] Kouji Segawa and Yoichi Ando, Phys. Rev. B **69**, 104521 (2004).

[12] Yoichi Ando, Y. Kurita, Seiki Komiya, S. Ono, and Kouji Segawa, Phys. Rev. Lett. **92**, 197001 (2004).

[13] Kouji Segawa and Yoichi Ando, Phys. Rev. Lett. **86**, 4907 (2001).

[14] A. N. Lavrov, Yoichi Ando, Kouji Segawa, and J. Takeya, Phys. Rev. Lett. **83**, 1419 (1999).

[15] X. F. Sun, Kouji Segawa, and Yoichi Ando, Phys. Rev. Lett. **93**, 107001 (2004).

[16] Y. S. Lee, Kouji Segawa, Yoichi Ando, and D. N. Basov, Phys. Rev. Lett. **94**, 137004 (2005).

[17] C. C. Homes, M. Reedyk, D. A. Crandles, and T. Timusk, Appl. Opt. **32**, 2976 (1993).

[18] D. N. Basov, A. V. Puchkov, R. A. Hughes, T. Strach, J. Preston, T. Timusk, D. A. Bonn, R. Liang, and W. N. Hardy, Phys. Rev. B **49**, 12165 (1994).

[19] D. N. Basov, B. Dabrowski, and T. Timusk, Phys. Rev. Lett. **81**, 2132 (1998).

[20] M. Dumm, D. N. Basov, Seiki Komiya, Yasushi Abe, and Yoichi Ando, Phys. Rev. Lett. **88**, 147003 (2002).

[21] Alternative interpretations of the finite-ω coherent modes involve scenarios emphasizing the proximity of the weakly doped phases to the Mott transition. P. A. Marchetti, G. Orso, Z. B. Su, and L. Yu, Phys. Rev. B **69**, 214514 (2004).

[22] T. Timusk and B. Statt, Rep. Prog. Phys. **62**, 61 (1999).

[23] C. C. Homes, T. Timusk, R. Liang, D. A. Bonn, and W. N. Hardy, Phys. Rev. Lett. **71**, 1645 (1993).

[24] D. N. Basov, T. Timusk, B. Dabrowski, and J. D. Jorgensen, Phys. Rev. B **50**, R3511 (1994).

[25] D. N. Basov, R. Liang, B. Dabrowski, D. A. Bonn, W. N. Hardy, and T. Timusk, Phys. Rev. Lett. **77**, 4090 (1996).

[26] A. V. Puchkov, D. N. Basov, and T. Timusk, J. Phys.: Condens. Matter **8**, 10049 (1996).

[27] D. N. Basov and T. Timusk (unpublished).

[28] T. Timusk and D. Tanner, in *Physical Properties of High Temperature Superconductors III*, edited by D. M. Ginsberg (World Scientific, Singapore, 1992), Chap. 5.

[29] M. A. Quijada, D. B. Tanner, R. J. Kelley, M. Onellion, H. Berger, and G. Margaritondo, Phys. Rev. B **60**, 14917 (1999).

[30] A. V. Puchkov, P. Fournier, T. Timusk, and N. N. Kolesnikov, Phys. Rev. Lett. **77**, 1853 (1996).

[31] D. N. Basov, E. J. Singley, and S. V. Dordevic, Phys. Rev. B **65**, 054516 (2002).

[32] J. P. Carbotte, E. Schachinger, and D. N. Basov, Nature (London) **401**, 354 (1999).

[33] D. Munzar, C. Bernhard, and M. Cardona, Physica C **312**, 121 (1999).

[34] J. Hwang, T. Timusk, and G. D. Gu, Nature (London) **427**, 714 (2004).

[35] A. Abanov, A. V. Chubukov, M. Eschrig, M. R. Norman, and J. Schmalian, Phys. Rev. Lett. **89**, 177002 (2002).

[36] P. B. Allen, Phys. Rev. B **3**, 305 (1971).

[37] S. V. Dordevic, E. J. Singley, D. N. Basov, S. Komiya, Y. Ando, E. Bucher, C. C. Homes, and M. Strongin, Phys. Rev. B **65**, 134511 (2002), and references therein.

[38] D. N. Basov, C. C. Homes, E. J. Singley, M. Strongin, T. Timusk, G. Blumberg, and D. van der Marel, Phys. Rev. B **63**, 134514 (2001).

[39] C. C. Homes, S. V. Dordevic, D. A. Bonn, Ruixing Liang, and W. N. Hardy, Phys. Rev. B **69**, 024514 (2004).

[40] C. O'Donovan and J. P. Carbotte, Phys. Rev. B **52**, 16208 (1995).

[41] J. Orenstein, Physica C **87**, 243 (2003).

[42] T. Holstein, Phys. Rev. **96**, 539 (1954).

[43] R. R. Joyce and P. L. Richards, Phys. Rev. Lett. **24**, 1007 (1970).

[44] B. Farnworth and T. Timusk, Phys. Rev. B **14**, 5119 (1976).

[45] G. A. Thomas, J. Orenstein, D. H. Rapkine, M. Capizzi, A. J. Millis, R. N. Bhatt, L. F. Schneemeyer, and J. V. Waszczak, Phys. Rev. Lett. **61**, 1313 (1988).

[46] M. R. Norman and H. Ding, Phys. Rev. B **57**, R11089 (1998).

[47] H. F. Fong, P. Bourges, Y. Sidis, L. P. Regnault, J. Bossy, A. Ivanov, D. L. Milius, I. A. Aksay, and B. Keimer, Phys. Rev. B **61**, 14773 (2000).

[48] Pengcheng Dai, H. A. Mook, R. D. Hunt, and F. Doğan, Phys. Rev. B **63**, 054525 (2001).

[49] P. D. Johnson, T. Valla, A. V. Fedorov, Z. Yusof, B. O. Wells, Q. Li, A. R. Moodenbaugh, G. D. Gu, N. Koshizuka, C. Kendziora, Sha Jian, and D. G. Hinks, Phys. Rev. Lett. **87**, 177007 (2001).

[50] A. Abanov and A. V. Chubukov, Phys. Rev. Lett. **83**, 1652 (1999).

[51] J. F. Zasadzinski, L. Ozyuzer, N. Miyakawa, K. E. Gray, D. G. Hinks, and C. Kendziora, Phys. Rev. Lett. **87**, 067005 (2001).

[52] A. Abanov and A. V. Chubukov, Phys. Rev. B **61**, R9241 (2000).

[53] A. Lanzara, P. V. Bogdanov, X. J. Zhou, S. A. Kellar, D. L. Feng, E. D. Lu, T. Yoshida, H. Eisaki, A. Fujimori, K. Kishio, J.-I. Shimoyama, T. Noda, S. Uchida, Z. Hussain, and Z.-X. Shen, Nature (London) **412**, 510 (2001); G.-H. Gweon, T. Sasagawa, S. Y. Zhou, J. Graf, H. Takagi, D.-H. Lee, A. Lanzara, *ibid.* **430**, 187 (2004).

[54] N. L. Wang, T. Timusk, J. P. Franck, P. Schweiss, M. Braden, and A. Erb, Phys. Rev. Lett. **89**, 087003 (2002).

[55] C. Bernhard, T. Holden, A. V. Boris, N. N. Kovaleva, A. V. Pimenov, J. Humlicek, C. Ulrich, C. T. Lin, and J. L. Tallon, Phys. Rev. B **69**, 052502 (2004).

[56] Pengcheng Dai, H. A. Mook, G. Aeppli, S. M. Hayden, and F. Doğan, Nature (London) **406**, 965 (2000).

[57] S. V. Dordevic, C. C. Homes, J. J. Tu, T. Valla, M. Strongin, P. D. Johnson, G. D. Gu, and D. N. Basov, Phys. Rev. B **71**, 104529 (2005).

[58] Pengcheng Dai, H. A. Mook, S. M. Hayden, G. Aeppli, T. G. Perring, R. D. Hunt, and F. Doğan, Science **284**, 1344 (1999).

[59] W. J. Padilla, Z. Q. Li, K. S. Burch, Y. S. Lee, K. J. Mikolaitis, and D. N. Basov, Rev. Sci. Instrum. **75**, 4710 (2004).

[60] S. Uchida, T. Ido, H. Takagi, T. Arima, Y. Tokura, and S. Tajima, Phys. Rev. B **43**, 7942 (1991).

[61] Y. Onose, Y. Taguchi, K. Ishizaka, and Y. Tokura, Phys. Rev. B **69**, 024504 (2004).

[62] A. Zimmers, J. M. Tomczak, R. P. S. M. Lobo, N. Bontemps, C. P. Hill, M. C. Barr, Y. Dagan, R. L. Greene, A. J. Millis, and C. C. Homes, Europhys. Lett. **70**, 225–231 (2005).

[63] N. L. Wang, G. Li, Dong Wu, X. H. Chen, C. H. Wang, and H. Ding, cond-mat/0410242 (unpublished).

[64] D. Pines and P. Nozieres, *The Theory of Quantum Liquids* (Benjamin, New York, 1996).

[65] S. V. Borisenko, A. A. Kordyuk, S. Legner, T. K. Kim, M. Knupfer, C. M. Schneider, J. Fink, M. S. Golden, M. Sing, R. Claessen, A. Yaresko, H. Berger, C. Grazioli, and S. Turchini, Phys. Rev. B **69**, 224509 (2004).

[66] S. V. Dordevic, E. J. Singley, J. H. Kim, M. B. Maple, Seiki Komiya, S. Ono, Yoichi Ando, T. Rõõm, Ruxing Liang, D. A. Bonn, W. N. Hardy, J. P. Carbotte, C. C. Homes, M. Strongin, and D. N. Basov, Phys. Rev. B **69**, 094511 (2004).

[67] A. Ino, C. Kim, M. Nakamura, T. Yoshida, T. Mizokawa, A. Fujimori, Z.-X. Shen, T. Kakeshita, H. Eisaki, and S. Uchida, Phys. Rev. B **65**, 094504 (2002).

[68] Andrea Damascelli, Zahid Hussain, and Zhi-Xun Shen, Rev. Mod. Phys. **75**, 473 (2003).

[69] D. van der Marel, H. J. A. Molegraaf, J. Zaaren, Z. Nussinov, F. Carbone, A. Damascelli, H. Eisaki, M. Greven, P. H. Kes, and M. Li, Nature (London) **425**, 271 (2003).

[70] Y. S. Lee, J. S. Lee, K. W. Kim, T. W. Noh, Jaejun Yu, Yunkyu Bang, M. K. Lee, and C. B. Eom, Phys. Rev. B **64**, 165109 (2001).

[71] E. W. Carlson, V. J. Emery, S. A. Kivelson, and D. Orgad, cond-mat/0206217 (unpublished).

[72] Michael Vershinin, Shashank Misra, S. Ono, Y. Abe, Yoichi Ando, and Ali Yazdani, Science **303**, 1995 (2004).

[73] T. Hanaguri, C. Lupien, Y. Kohsaka, D.-H. Lee, M. Azuma, M. Takano, H. Takagi, J. C. Davis, Nature (London) **430**, 1001 (2004).

[74] G. Grüner, *Density Waves in Solids* (Addison-Wesley, Reading, MA, 1994).

[75] E. Dagotto, Rev. Mod. Phys. **66**, 763 (1994) M. M. Zemljic and P. Prelovsek, cond-mat/0504640 (unpublished).

[76] J. Lorenzana and G. A. Sawatzky, Phys. Rev. Lett. **74**, 1867 (1995); J. Lorenzana and G. A. Sawatzky, Phys. Rev. B **52**, 9576 (1995).

[77] V. J. Emery and S. A. Kivelson, Physica C **209**, 597 (1993).

[78] V. J. Emery and S. A. Kivelson, Phys. Rev. Lett. **74**, 3253 (1995).

[79] S. A. Kivelson and D. Stroud (private communications).

[80] S. Lupi, M. Capizzi, P. Calvani, B. Ruzicka, P. Maselli, P. Dore, and A. Paolone, Phys. Rev. B **57**, 1248 (1998); S. Lupi, P. Maselli, M. Capizzi, P. Calvani, P. Giura, and P. Roy, Phys. Rev. Lett. **83**, 4852 (1999).

[81] J.-H. Eom, S.-S. Lee, K.-S. Kim, and Sung-HoSuck Salk, Phys.

Rev. B **70**, 024522 (2004), and references therein.

[82] A. J. Leggett, Proc. Natl. Acad. Sci. U.S.A. **96**, 8365 (1999).

[83] Misha Turlakov and Anthony J. Leggett, Phys. Rev. B **67**, 094517 (2003).

[84] H. J. A. Molegraaf, C. Presura, D. van der Marel, P. H. Kes, and M. Li, Science **295**, 2239 (2002); M. Rubhausen, A. Gozar, M. V. Klein, P. Guptasarma, and D. G. Hinks, Phys. Rev. B **63**, 224514 (2001).

[85] Hae-Young Kee, Steven A. Kivelson, and G. Aeppli, Phys. Rev. Lett. **88**, 257002 (2002).

[86] Ilya Eremin, Dirk K. Morr, Andrey V. Chubukov, Karl Bennemann, and Michael R. Norman, cond-mat/0409599 (unpublished).

[87] Masatoshi Imada, Atsushi Fujimori, and Yoshinori Tokura, Rev. Mod. Phys. **70**, 1039 (1998).

[88] Arun Paramekanti, Mohit Randeria, and Nandini Trivedi, Phys. Rev. Lett. **87**, 217002 (2001).